Clinical Translational Evaluation of Al18F-NOTA-FAPI for Fibroblast Activation Protein Targeted Tumour Imaging

Shuailiang Wang
Institute of Medical Technology, Peking University Health Science Center
Xin Zhou
Peking University Cancer Hospital & Institute
Xiaoxia Xu
Peking University Cancer Hospital & Institute
Jin Ding
Peking University Cancer Hospital & Institute
Song Liu
Peking University Cancer Hospital & Institute
Xingguo Hou
Peking University Cancer Hospital & Institute
Nan Li
Peking University Cancer Hospital & Institute
Hua Zhu
Peking University Cancer Hospital & Institute
Zhi Yang (pekyz@163.com)
Peking University Cancer Hospital & Institute https://orcid.org/0000-0003-2084-5193

Research Article

Keywords: Fibroblast activation protein, A118F, PET/CT, Tumour imaging, Clinical translational evaluation

Posted Date: February 24th, 2021

DOI: https://doi.org/10.21203/rs.3.rs-231262/v1

Clinical Translational Evaluation of Al^{18}F-NOTA-FAPI for Fibroblast Activation Protein Targeted Tumour Imaging

Shuailiang Wang[1,2], Xin Zhou[2], Xiaoxia Xu[2], Jin Ding[2], Song Liu[2], Xingguo Hou[2], Nan Li[2], Hua Zhu[2*], Zhi Yang[1,2*]

[1]Institute of Medical Technology, Peking University Health Science Center, Beijing 100191, China; [2]Key Laboratory of Carcinogenesis and Translational Research (Ministry of Education/Beijing), Department of Nuclear Medicine, Peking University Cancer Hospital & Institute, Beijing 100142, China.

Corresponding author:

Hua Zhu, Peking University Cancer Hospital & Institute, No. 52 Fu-Cheng Rd., Beijing, 100142, China. E-mail: zhuhuananjing@163.com

Zhi Yang, Peking University Cancer Hospital & Institute, No. 52 Fu-Cheng Rd., Beijing, 100142, China. E-mail: pekyz@163.com

Abstract

Purpose In this study, a novel Al^{18}F-NOTA-FAPI probe was developed for fibroblast activation protein (FAP) targeted tumour imaging, which was available to achieve curie level radioactivity by automatic synthesizer. The tumour detection efficacy of Al^{18}F-NOTA-FAPI was further validated both in preclinical and clinical translational studies.

Methods The radiolabeling procedure of Al^{18}F-NOTA-FAPI was optimized. Cell uptake and competitive binding assay were completed with U87MG and A549 cell lines, to evaluate the affinity and specificity of Al^{18}F-NOTA-FAPI probe. The biodistribution, pharmacokinetics, radiation dosimetry and tumour imaging efficacy of Al^{18}F-NOTA-FAPI probe were researched with healthy Kunming (KM) and/or U87MG model mice. After the approval of ethical committee, Al^{18}F-NOTA-FAPI probe was translated into clinical for the PET/CT imaging of first 10 cancer patients.

Results The radiolabeling yield of Al^{18}F-NOTA-FAPI was 33.8 ± 3.2% through manually operation (n = 10), with the radiochemical purity over than 99% and the

specific activity of 9.3-55.5 MBq/nmol. Whole body effective dose of Al^{18}F-NOTA-FAPI was estimated to be 1.24E-02 mSv/MBq, lower than several other FAPI probes (^{68}Ga-FAPI-04, ^{68}Ga-FAPI-46 and ^{68}Ga-FAPI-74). In U87MG tumour bearing mice, Al^{18}F-NOTA-FAPI showed good tumor detection efficacy from the results of micro PET/CT imaging and biodistribution studies. In organ biodistribution study of human patients, Al^{18}F-NOTA-FAPI showed lower SUVmean than 2-[^{18}F]FDG in most organs, especially in liver (1.1 ± 0.2 vs. 2.0 ± 0.9), brain (0.1 ± 0.0 vs. 5.9 ± 1.3), and bone marrow (0.9 ± 0.1 vs. 1.7 ± 0.4). Meanwhile, Al^{18}F-NOTA-FAPI do not show extensive bone uptakes, and was able to find out more tumour lesions than 2-[^{18}F]FDG in the PET/CT imaging of several patients.

Conclusion Al^{18}F-NOTA-FAPI probe was successfully fabricated and applied in fibroblast activation protein targeted tumour PET/CT imaging, which showed excellent imaging quality and tumour detection efficacy in U87MG tumour bearing mice as well as in human cancer patients.

Trial registration: Chinese Clinical Trial Registry ChiCTR2000038080. Registered 09 September 2020. http://www.chictr.org.cn/showproj.aspx?proj=61192

Keyword Fibroblast activation protein; Al^{18}F; PET/CT; Tumour imaging; Clinical translational evaluation

Declarations

Funding This work was supported by National Natural Science Foundation of China projects No. 81871386 and 81871387, Yangfan project No. ZYLX201816, Dengfeng project No. DFL20191102, and Science Foundation of Peking University Cancer Hospital-2020-18.

Conflicts of interest The authors declare that they have no conflict of interest.

Availability of data and material Not applicable.

Code availability Not applicable.

Authors' contributions ZY and HZ conceived and designed this research. SW was responsible to all the experiments, data collection and analysis, and also wrote the manuscript. XZ and XX were responsible to the recruitment of patients and image analysis. JD, SL and XH were involvode in the preparation of radiopharmaceuticals and also took part in most of the animal experiments. All of the authors joined in the embellishment of the article.

Ethics approval All procedures involving human participants were carried out in accordance with the Ethics Committee of Peking University Cancer Hospital (2019 KT95), and registered in Chinese Clinical Trial Registry (ChiCTR2000038080). All animal studies were performed according to a protocol approved by the Peking University Cancer Hospital Animal Care and Use Committee.

Consent to participate Written informed consents were obtained from all participants included in the study.

Consent for publication Not applicable.

Clinical Trial Registration This study was approved by the Ethics Committee of Peking University Cancer Hospital (2019 KT95), and registered in Chinese Clinical Trial Registry (ChiCTR2000038080).

Acknowledgments

We gratefully appreciate all the chemists, nurses, and technicians from the Department of Nuclear Medicine, Peking University Cancer Hospital for their contributions to tracer administration and PET/CT imaging.

Introduction

Fibroblast activation protein (FAP) is a type II transmembrane glycoprotein consisting of 760 amino acids, which belongs to the serine protease family and is selectively expressed in the stroma fibroblasts associated with epithelial cancers [1]. Reactive tumour stroma or fibrosis generally presents with increased number of activated fibroblasts that usually express FAP, whereas normal stroma in most adult organs only

contains a small number of quiescent or resting fibroblasts with low or undetectable FAP expression, making FAP a novel metabolic target in cancer theranostics [2, 3]. Till now, plenty of therapies targeting FAP have been explored, including FAP inhibitors [4], peptide drug complexes [5, 6], antibodies [7], CAR-T cell therapy [8], vaccines [9] and tumour immunotherapy [10].

Especially in recent several years, (4-Quinolinoyl)glycyl-2-cyanopyrrolidine based organic small molecules that exhibited excellent affinity with FAP [11], known as FAP inhibitor (FAPI), have been radiolabeled with different radionuclides including ^{68}Ga, ^{90}Y, ^{99m}Tc, ^{64}Cu and ^{225}Ac, and have been translated into clinical for the nuclear imaging and radionuclide therapy of various types of cancer [12-15]. Earlier study indicated that several highly prevalent cancers showed remarkably high uptake and image contrast on ^{68}Ga-FAPI PET/CT imaging [13]. More importantly, in contrast to 2-[^{18}F]FDG, no diet or fasting is required in preparation for the ^{68}Ga-FAPI examination, and the image acquisition in ^{68}Ga-FAPI imaging can be potentially started much earlier than 2-[^{18}F]FDG imaging [16].

However, ^{68}Ga-FAPI PET/CT imaging suffered the disadvantage of radionuclide supply, since ^{68}Ga was usually eluted from ^{68}Ge-^{68}Ga generator, one single synthesis would only achieve a small amount of radiopharmaceutics avaliable to 2-4 patients. Meanwhile, the supply of ^{68}Ga-FAPI to distant centres that requiring this probe would be restricted because of the short half-life of ^{68}Ga ($t_{1/2}$ = 68 min). Remolding of ^{68}Ga-FAPI into ^{18}F radiolabeled probes would fundamentally resolve its intrinsic disadvantages mentioned above, in consideration of the longer half-life of ^{18}F ($t_{1/2}$ = 109.8 min) and the availability of ^{18}F from cyclotron that owned by many medical centres. Additionally, the lower positron energy of ^{18}F (Emean = 0.25 MeV vs. 0.83 MeV of ^{68}Ga) rendered it a shorter positron range than ^{68}Ga (0.6 mm vs. 3.5 mm), which would result in a higher spatial resolution on PET/CT imaging [17]. Most recently, two ^{18}F radiolabeled FAPI probes has been reported, namely ^{18}F-FAPI-74 and [^{18}F]FGlc-FAPI, respectively [18, 19]. Both of this two probes showed excellent tumour imaging efficacy, however, the structure of this novel Al^{18}F-NOTA-FAPI probe was different from them.

Herein, we report the rapid and efficient radiolabeling strategy of a novel Al^{18}F-NOTA-FAPI probe and carried out its preclinical investigations. Furthermore, Al^{18}F-NOTA-FAPI is translated into clinical application for the PET/CT imaging of patients with different types of cancer, and its imaging efficacy is compared with 2-[^{18}F]FDG.

Materials and methods

Chemicals and reagents

Metal basis chemicals used in this study include the following: potassium hydrogen phthalate (KHP) was purchased from Acros Organics (USA), anhydrous aluminum chloride ($AlCl_3$) and sodium acetate were purchased from Alfa Aesar (China) Chemicals Co. Ltd. Reagents including ethanol and acetonitrile were purchased from Honeywell International Inc (USA), trifluoroacetic acid (TFA) was purchased from Shanghai Aladdin Biochemical Technology Co., Ltd (China). All chemicals and reagents were applied directly without further purification. NOTA-FAPI precursor was purchased from HUAYI Co. Ltd (China). Reagents including phosphate buffer saline (PBS), cell culture medium, fetal bovine serum (FBS), penicillin-streptomycin solution (PS), Glutamax, non-essential amino acid (NEAA) and trypsin for cell culturing and following experiments were obtained from Gibco (Thermo Fisher Scientific, China).

Cell culture and tumour models

U87MG and A549 cancer cell lines were obtained from National Collection of Authenticated Cell Cultures. U87MG cells were cultivated in Dulbecco modified Eagle medium (DMEM high glucose) containing 10% FBS, 1% PS, 1% Glutamax and 1% NEAA at 37 ºC in 5% carbon dioxide. A549 cells were cultivated in Roswell Park Memorial Institute (RPMI 1640) medium containing 10% FBS, 1% PS at 37 ºC in 5% carbon dioxide.

U87MG and A549 tumour bearing BALB/c Nude mice (6-8 weeks, female, 16-20 g) were purchased from Beijing Vital River Laboratory Animal Technology Co. Ltd (China). Mice of specific pathogen free (SPF) grade were breeding in individual ventilated cages (IVC) with free available of food and water. Tumour on the right flank

of mice were allowed to reach an volume of approximately 0.5-0.8 cm in diameter, and animals were further allpied for following imaging and in vivo biodistribution experiments. All animal experiments were completed in accordance with relavant guides and regulations of Beijing Cancer Hospital.

Radiopharmaceutical preparation

As shown in Fig. 1, radiolabeling of $Al^{18}F$-NOTA-FAPI was completed based on a previous reported method with some modifications [20]. Briefly, $^{18}F^-$ was produced from HM-20 medical cyclotron (Sumitomo Corporation, Japan), loaded on QMA cartridge (Waters Corporation, USA) and further eluted with saline (0.3-0.5 mL). For the radiolabeling, $^{18}F^-$ in saline (0.1 mL, 555-3330 MBq) was mixed with $AlCl_3$ (6 μL, 2 mM) and KHP (6 μL, 0.5 M) for 5 min under room temperature to form the $[Al^{18}F]^{2+}$ conjugate, NOTA-FAPI precursor (5 μL, 4 mM) was further added to the reaction system and heated at 110 °C for 15 min. After that, the reaction system was diluted with 5 mL of ultrapure water and purified with Sep-Pak Light C18 cartridge (Waters Corporation, USA). Final product was formulated through the elution of C18 cartridge with 0.5 mL of 80% ethanol and 6 mL of saline consecutively, and further passed through a 0.2 μm syringe filter (Pall Corpotation, USA). The radiochemical purity of $Al^{18}F$-NOTA-FAPI was analyzed by a radio high performance liquid chromatograph (1200 Series, Agilent, USA) with gradient elution: 0-3 min, 95% water (0.1% TFA) + 5% acetonitrile (0.1% TFA); 18 min, 5% water (0.1% TFA) + 95% acetonitrile (0.1% TFA); 20 min, 95% water (0.1% TFA) + 5% acetonitrile (0.1% TFA).

Stability and partition coefficient

The in vitro stability of $Al^{18}F$-NOTA-FAPI was assessed in saline and 5% human serum albumin (HSA) for 1 h, 2 h and 4 h with radio-HPLC. For in vivo stability assessment, KM mice (female, 18-20 g, n = 3) was administered with approximately 37 MBq of $Al^{18}F$-NOTA-FAPI intravenously, urine and blood was collected at 10 min, 0.5 h and 1 h post-injection, radiochemical purity of $Al^{18}F$-NOTA-FAPI in the urine and blood of mice was analyzed with radio-HPLC.

The octanol-water partition coefficient of $Al^{18}F$-NOTA-FAPI was detected by mixting

10 μL of purified $Al^{18}F$-NOTA-FAPI with 590 μL of PBS (0.1 M, pH 7.4) and 600 μL of octanol in a 1.5 mL tube (n = 5). The mixture was vortexed for 3 min and further centrifugated at 3000 × rpm for 5 min, a small portion (10 μL) was removed from each phase and further counted with a γ counter (Wizard II, Perkin Elmer Inc., Germany). The partition coefficient was calculated as the counts in octanol divided by the counts in phosphate buffered saline, the value was expressed as $logD_{7.4}$ (mean ± SD).

Cell uptake and competitive binding assay

For cell uptake experiment, cells were seeded in 24-well plates overnight (2×10^5 per well). Cells were washed with PBS (pH 7.4, 0.01 M) twice and replaced with fresh medium without FBS. Cells were incubated with 74 kBq of $Al^{18}F$-NOTA-FAPI in 1 mL of medium for 10, 30 and 60 min at 37 ºC. In the blocking group, an extra amount (1 μg/well) of non-radiolabeled precursor was added. After that, cells were washed twice with cold PBS (pH 7.4, 0.01 M) and lysed with 200 μL of NaOH (0.1 M). The lysate was collected and counted with a γ counter. The results were normalized to 1×10^6 cells and expressed as percentage of added dose (%AD/10^6 cell). The experiment was repeated three times for each time point.

For competitive binding assay, different concentrations of unlabeled precursor (0.1 nM to 10 μM) was added to cells with fixed activity of radiolabeled $Al^{18}F$-NOTA-FAPI (74 kBq/well). The cells were incubated at 37 ºC for 30 min, washed with cold PBS (pH 7.4, 0.01 M) for two times and further lysed with 200 μL of NaOH (0.1 M). The lysate was collected and counted with a γ counter. The experiment was repeated three times for each concentration. The IC_{50} of NOTA-FAPI was acquired using the non-linear curve fitting of GraphPad Prism 8.3.0 software (GraphPad Software, San Diego, CA, USA).

Small animal biodistribution and pharmacokinetics study

For animal biodistribution study, KM mice (female, 4 weeks, 18-20 g) were devided into 5 groups (n = 3) and injected with $Al^{18}F$-NOTA-FAPI (200 μL, 1.85 MBq/per mouse) intravenously, 1% injected dose of $Al^{18}F$-NOTA-FAPI was prepared and set as contrast. At 5 min, 30 min, 1 h, 2 h, 4 h post-injection, KM mice were sacrificed after

anesthetization, organs of interest were collected, weighted, and counted with a γ counter. As a standard, 10 samples of 1% injected dose were taken from the injection and counted. The biodistribution of Al^{18}F-NOTA-FAPI in different organs of KM mice was expressed as percentage injected dose per gram (%ID/g, mean ± SD).

For biodistribution of Al^{18}F-NOTA-FAPI in tumour bearing mice, U87MG and A549 (negative control) tumour bearing mice were grouped and injected intravenously with 200 μL of radiotracer (~ 1.11 MBq). At 1 h post injtection, mice were anesthetized and sacrificed, blood samples and organs of interest were collected, weighted and counted with a γ counter. For the block group, mice were co-injtected with 20 nmol (15.4 μg) of non-radiolabeled FAPI precursor.

Pharmacokinetics study was accoplished using female KM mice (n = 5). Briefly, each mouse was intravenously injected with 3.7 MBq of Al^{18}F-NOTA-FAPI. A small portion of blood was acqiured through the orbital venous of mice at 1 min, 3 min, 5 min, 10 min, 15 min, 30 min, 45 min, 60 min, 90 min, 120 min, 180 min and 240 min post-injection. The blood samples were weighted before counted using a γ counter. The results were calculated as percentage injected dose per gram (%ID/g, mean ± SD).

Radiation dosimetry estimation

The internal radiation dosimetry of Al^{18}F-NOTA-FAPI probe in adult female patients was estimated according to the biodistribution results in KM mice. Area under the time-activity curves (AUCs) of different organs were calculated using GraphPad Prism 8.3.0, and the results were further analyzed using OLINDA/EXM software (version 1.0; Hermes Medical Solutions AB) to estimate the absorbed dose of each organ, as well as the effective dose of whole body.

Micro PET/CT imaging in mice bearing U87MG and A549 xenograft

Tumour bearing BALB/c Nude mice were injected with 200 μL of Al^{18}F-NOTA-FAPI (~7.4 MBq), at 1 h post injection, mice were anesthetized and placed on the imaging bed to perform the micro PET-CT imaging (SuperNova, PINGSENG Healthcare, China). PET images were acquired for 10 minutes and reconstruted with attenuation correction based on the CT data (CT-AC reconstruction). Regions of interest (ROI)

were drawn on the CT images and further mapped on PET, SUVmax of tumour and muscle were calculated and referred to as tumour to muscle ratio. In the block group, mouse were co-injected with an extra amount (20 nmol) of non-radiolabeled precursor.

Patient enrollment

The clinical translational study of Al^{18}F-NOTA-FAPI was approved by the Ethics Committee (approval No. 2019KT95) of Beijing Cancer Hospital, and registered in Chinese Clinical Trial Registry (ChiCTR2000038080), all patients enrolled in this study have signed a written informed consent. The include criteria were as follows, 18 to 75 years old cancer patients or suspected cancer patients, ability to provide a written informed consent, normal liver and kidney function. The exclusion criteria included the following: liver and renal dysfunction, pregnancy or current lactation and patients that suffered psychiatry disease or claustrophobia.

PET/CT imaging in cancer patients

For tracer administration, all patients received intravenously injection through the elbow or opisthenar vein with the radioactivity ranged from 173.5 MBq to 256.8 MBq. At 60-90 min post-injection, patients were required for urination and received static PET/CT scan (Siemens, Erlangen, Germany) from the top of the skull to the middle of the femur. A Siemens workstation (syngo.via Client 4.1) was used for image processing. Two experienced nuclear medicine physicians independently reviewed all images, and any discordant results were resolved by consensus. The SUVmax and SUVmean values of tumour lesions as well as normal organs were quantified by delineation of ROI directly on the PET/CT iamges.

RESULTS

Radiopharmaceutical preparation

The synthetic procedure of Al^{18}F-NOTA-FAPI was presented in Fig. 1, and the molecular structures of this probe as well as earlier reported [^{18}F]FGlc-FAPI were compared directly. This study evaluated several parameters which might influence the

radiolabeling yield, including the amount of $AlCl_3$ (2 mM), KHP (0.5 M) and precursor (4 mM), as well as the temperature and raction volume. As shown in Fig. S1, all parameters exhibited significant impact on radiolabeling yield. Meanwhile, the optimal radiolabeling parameters are as follows, both the volumes of $AlCl_3$ and KHP were 6 μL, the amount of precursor was 5 μL, the volume of $^{18}F^-$ ions in saline was 100 μL. The reaction mixture was heated at 110 ^oC for 15 min, and further purified with Sep-Pak Light C18 cartridge. The highest radiolabeling yield under the optimal reaction conditions, appoximately 36.5% can be achieved under manual operation (33.8 ± 3.2% on average, n = 10). The specific activity of $Al^{18}F$-NOTA-FAPI was around 9.3-55.5 MBq/nmol, according to the activity of $^{18}F^-$ ions added. Radiochemical purity of the final product was higher than 99%. Furthermore, $Al^{18}F$-NOTA-FAPI with much higher activity (> 100 mCi) can be achieved under automatic synthesis with this optimal reaction condition.

Stability and partition coefficient

Both the in vitro and in vivo stability of $Al^{18}F$-NOTA-FAPI were determined with radio-HPLC. The radiopharmaceutical showed excellent stability in vitro, including in saline and 5% HSA, kept almost intact within 4 h (radiochemical purity > 95%, Fig. S2). Furthermore, the stability of $Al^{18}F$-NOTA-FAPI was also perfect in vivo, although slightly compromised compared with its in vitro stability. Within 1 h post injection, radiochemical purity of the radiopharmaceutical were higher than 90%, both in blood and urine. Meanwhile, the partition coefficient of $Al^{18}F$-NOTA-FAPI was calculated as $logD_{7.4} = -1.88 \pm 0.01$, with the majority of radioactivity concentrared in the water phase (>98%), indicating the superior hydrophilicity of $Al^{18}F$-NOTA-FAPI.

Cell uptake and IC_{50} of NOTA-FAPI

As shown in Fig. 2a, in FAP positive U87MG cells, highest uptake of $Al^{18}F$-NOTA-FAPI was observed at 10 min (2.13 ± 0.17 AD%), which can be blocked by the adding of excess non-radiolabeled precursor (0.28 ± 0.03 AD%), indicating the specific binding between $Al^{18}F$-NOTA-FAPI and fibroblast activation protein. The uptake of $Al^{18}F$-NOTA-FAPI in U87MG cells decreased from 10 min to 2 h. While in FAP

negative A549 cells, much lower and stable uptake of the radiopharmaceutical was observed at all time points (Fig. S3). Moreover, the IC_{50} of NOTA-FAPI was calculated to be 1.73 ± 0.93 nM (Fig. 2b), which was lower than several other FAPI probes (Table S1), indicating the high affinity between NOTA-FAPI and FAP.

Small animal biodistribution and pharmacokinetics study

In KM mice, the tracer showed rapid clearence through the kidney, with extremely low uptake in most normal organs including liver, lung, spleen and brain (Fig. 3a). At 1 h post injection, the highest uptake was observed in the gallbladder (17.83 ± 2.92%ID/g), followed by the bone (6.34 ± 0.98%ID/g) and muscle (1.25 ± 0.47%ID/g). The tracer uptake in most organs decrased rapidly along with time, except in the bone and gallbladder. A comparison of the biodistribution at 1 h post injection in KM mice between ^{68}Ga-FAPI and Al^{18}F-NOTA-FAPI was presented in Tabel 1. In all tested organs, the uptake of Al^{18}F-NOTA-FAPI was lower than ^{68}Ga-DOTA-FAPI-04, especially in the spleen, stomach wall and muscle (Fig. S4).

Furthermore, pharmacokinetics study of Al^{18}F-NOTA-FAPI in mice provided conclusive evidence for its rapid clearance from body. As shown in Fig. 3b and equation (1), pharmacokinetics of Al^{18}F-NOTA-FAPI followed two phase decay in mice, with an extremely short biodistribution half life of only 1.583 min, and half life of the elimination phase was only 14.75 min.

$$Ct = 2.46 + 13.82 \times e^{-0.44t} + 6.84 \times e^{-0.05t} \quad \text{.....(1)}$$

In U87MG tumour bearing xenografts, Al^{18}F-NOTA-FAPI showed extremely high accumulation in the tumour region (35.29 ± 1.00 %ID/g) and low uptake in most organs at 1 h post-injection, as shown in Fig. 4a. The uptake of Al^{18}F-NOTA-FAPI in the tumour was slightly higher than ^{68}Ga-DOTA-FAPI-04 both at 1 h and 4 h post-injection (Fig. 4b), and the uptake can be almost completely blocked (0.50 ± 0.11 %ID/g, $p < 0.0001$) by the adding of non-radiolabeled NOTA-FAPI. In A549 xenograft mice, the uptake of Al^{18}F-NOTA-FAPI in the tumour tissue was much lower, only reached 3.28 ± 0.66 %ID/g (Fig. S5). Al^{18}F-NOTA-FAPI showed relatively high uptake in the bone structure, both in U87MG (5.25 ± 0.68 %ID/g) and A549 (6.77 ± 0.93 %ID/g) tumour

bearing mice. However, the uptake in bone can be lowered (3.27 ± 0.28 %ID/g) by co-injection with non-radiolabeled NOTA-FAPI in U87MG tumour bearing mice ($p < 0.01$, Figure 4a). Alike ^{68}Ga-DOTA-FAPI-04 (Fig. S6), the retention of Al^{18}F-NOTA-FAPI in the tumour was not satisfied, with a decreasement of 33.72% from 1 h to 4 h post-injection.

Radiation dosimetry estimation

The internal radiation dosimetry in adult female patients was estimated based on the biodistribution results in KM mice. As shown in Tabel 2, most organs exhibited low absorbed dose as well as effective dose. The osteogenic cell had the highest absorbed dose (2.47E-02 mGy/MBq), followed by the red marrow (1.80E-02 mGy/MBq) and small intestine wall (1.54E-02 mGy/MBq). The whole body effective dose of Al^{18}F-NOTA-FAPI was calculated to be 1.24E-02 mSv/MBq.

Small animal PET/CT imaging

In A549 tumour bearing mice, no significant uptake of Al^{18}F-NOTA-FAPI was observed at the tumour region (SUVmax = 0.87), the tracer showed rapid clearence from body, with only high uptake in the gallbladder was noticed. However, in U87MG tumour xenografts, the tumour showed extremely high uptake of Al^{18}F-NOTA-FAPI (SUVmax = 3.53), meanwhile, high uptake in the gallbladder was also noticed. Interestingly, high uptake of Al^{18}F-NOTA-FAPI in the tumour region of U87MG xenografts can be almost totally blocked by co-injection of non-radiolabeled FAPI precursor, while most of the injected radiopharmaceutics were excreted through the biliary and intestine tract, indicating the specific uptake of Al^{18}F-NOTA-FAPI in the tumour area. (Fig. 5a-c). Futhermore, immunohistochemical staining results indicating high expression of FAP in U87MG xenograft but not in A549 tumour xenograft (Fig. 5d and 5e).

PET/CT imaging in cancer patients

Al^{18}F-NOTA-FAPI was successfully translated into clinical imaging of cancer patients with various tumour types, including lung cancer, pancreas cancer, colorectal cancer, prostate cancer and lymphoma patients (Table 3). In most normal organs of patients,

the SUVmean values in Al^{18}F-NOTA-FAPI PET/CT imaging were lower than that in 2-[^{18}F]FDG PET/CT imaging, especially in the liver (1.1 ± 0.2 vs. 2.0 ± 0.9), brain (0.1 ± 0.0 vs. 5.9 ± 1.3), spleen (0.7 ± 0.1 vs. 1.8 ± 0.4) and bone marrow (0.9 ± 0.1 vs. 1.7 ± 0.4) (Fig. 6a). However, the SUVmean of pancreas (3.0 ± 2.0 vs. 1.4 ± 0.4), muscle (1.6 ± 0.4 vs. 0.7 ± 0.1), submaxillary gland (3.5 ± 1.5 vs. 1.6 ± 0.5) and parotid gland (1.8 ± 0.7 vs. 0.9 ± 0.2) were higher in Al^{18}F-NOTA-FAPI PET/CT imaging than 2-[^{18}F]FDG PET/CT. The SUVmean of gallbladder was high in Al^{18}F-NOTA-FAPI PET/CT imaging (7.6 ± 10.5) of several but not all patients, which was consistently low in 2-[^{18}F]FDG PET/CT imaging (0.8 ± 0.4). In Al^{18}F-NOTA-FAPI PET/CT imaging, patients showed higher tumor/spleen and tumor/brain SUVmean ratios than 2-[^{18}F]FDG PET/CT imaging, as shown in Fig. 6b. Meanwhile, the SUVmax and SUVmean values were compared between Al^{18}F-NOTA-FAPI and 2-[^{18}F]FDG PET/CT imaging, as shown in Fig. S7, where no siginificant differences were noticed. The SUVmax and SUVmean values in the primary tumour lesions of individual patient were presented in Table S3.

Fig. 7 shows the representative images of a female pancreas cancer patient (64 years old) underwent Al^{18}F-NOTA-FAPI PET/CT imaging. The tumour lesion in the pancreas showed low uptake in 2-[^{18}F]FDG PET/CT imaging (SUVmax = 2.7, Fig. 7a-c), while in the Al^{18}F-NOTA-FAPI PET/CT imaging, the lesion showed extremely high uptake of radiotracer (SUVmax = 36.3, Fig. 7d-f). Furthermore, plenty of metastatic lymph nodes in the abdomen of this patient were clearly visualized in Al^{18}F-NOTA-FAPI PET/CT imaging, while not obvious in 2-[^{18}F]FDG PET/CT imaging. Fig. 8 shows another representative images of a lung cancer patient. The 59 years old female patient was diagnosed with a nodule in the superior lobe of left lung, which showed inappreciable uptake of 2-[^{18}F]FDG (SUVmax = 1.3, Fig. 8a-c). However, in Al^{18}F-NOTA-FAPI PET/CT imaging, the nodule was further validated as a malignancy lesion with relatively high uptake of Al^{18}F-NOTA-FAPI (SUVmax = 6.6, Fig. 8d-f). Interestingly, unlike the high uptake of Al^{18}F-NOTA-FAPI in the gallbladder in animal micro-PET/CT imaging, such phenomenon was not validated in some human patients, and the tracer uptake in the bone of human patients was negligible.

Discussion

Fibroblast activation protein targeted tumour imaging strategy developed rapidly in recent several years, especially utilizing FAP specific small molecule inhibitors. Although plenty of work needs to be further finished, FAPI has been deemed the most competitive radiotracer with ^{18}F-FDG in clinical tumour PET/CT imaging, because of its fast clearance from body, universality in the diagnosis of various types of cancer, and high tumour to background ratio. As we have successfully fabricated the Al^{18}F labeled PSMA ligand for tumour detection [20], it is also convenient to translate the ^{68}Ga-DOTA-FAPI into Al^{18}F-NOTA-FAPI probe. In this study, we investigated both the preclinical and clinical utilization of Al^{18}F-NOTA-FAPI probe, which showed great significance in the PET/CT imaging of cancer patients.

Compared with ^{68}Ga-FAPI, Al^{18}F-NOTA-FAPI showed faster clearance from body in mice biodistribution, rendered lower uptake in most normal organs. Meanwhile, the lower effective dose of Al^{18}F-NOTA-FAPI (1.24E-02 mSv/MBq) calculated in this study might also ascribe to its faster clearance. The effective dose of Al^{18}F-NOTA-FAPI was almost the same with ^{18}F-FAPI-74 (0.014 mSV/MBq) reported earlier, which contains a NOTA chelator and can also be radiolabeled with ^{18}F-AlF[18]. Although the structure of FAPI-74 was not public yet, its molecular weight was reported to be 735.8 g/mol, different from the probe (mw. 771.82) utilized in this study.

The high uptake in the gallbladder of mice was a characteristic of Al^{18}F-NOTA-FAPI, since such phenomenon was not noticed in ^{68}Ga-FAPI biodistribution. This can be ascribed to the higher lipophilicity of Al^{18}F-NOTA-FAPI, since the $LogD_{7.4}$ of Al^{18}F-NOTA-FAPI was calculated to be -1.88 ± 0.01, bigger than the $LogD_{7.4}$ of ^{68}Ga-DOTA-FAPI-04 (-2.87 ± 0.02). High accumulation of radiopharmaceutics in the bone of mice was appreciable, which was validated by small animal PET/CT imaging, especially in the shoulder joints, knee joints, skull and the spine of mice, which might be the explanation of the high absorbed dose and effective dose in osteogenic cells and red marrow, respectively. Such phenomenon was also noticed in previous study with the [^{18}F]FGlc-FAPI probe, which might because of the relatively high expression of FAP

in the osteoblast and bone marrow stem cells (BMSC) of mice, hence the high accumulation of FAPI probe in the skeleton of mice was ascribed to physiological uptake [19].

FAP was expressed primarily on the cancer associated fibroblasts but not on tumour cells, only several cancer cell lines showed high expression of FAP, including several glioblastoma cell line [21]. Indeed, much higher tumour cell uptake of Al^{18}F-NOTA-FAPI in U87MG cell line was noticed, compared with FAP low expressed A549 cell line in vitro. Since the uptake of Al^{18}F-NOTA-FAPI in U87MG cells can be blocked by extra adding of non-radiolabeled precursor, the specific binding between the radiopharmaceutical and FAP can be thus confirmed. Interestingly, the highest uptake of Al^{18}F-NOTA-FAPI in U87MG cells was observed at 10 min, and decreased in the following 2 hours, which was not reported by previous studies. We ascribe this to the rapid binding of Al^{18}F-NOTA-FAPI with FAP and internalization in U87MG cells, since the IC_{50} of NOTA-FAPI was lower than any previously reported FAPI probes (Table S2) [12, 22].

Also, from the biodistribution analysis results of tumour bearing mice, tracer uptake in U87MG xenografts was approximate 10 folds higher than that in A549 xenografts, while no significant differences were noticed in most normal organs. Meanwhile, in small animal PET/CT imaging, extremely high uptake of Al^{18}F-NOTA-FAPI in the tumour region of U87MG xenograft can be observed, the tumour-to-muscle SUVmax ratio was 23.5, much higher than A549 mice xenograft (tumour/muscle SUVmax ratio = 6.2). While in the mice co-injected with non-radiolabeled NOTA-FAPI, most of the radioactivity was accumulated in the gallbladder and intestine, further indicated the specific binding of Al^{18}F-NOTA-FAPI to FAP. Moreover, in this study, the immunohistological chemistry staining of both A549 and U87MG tumours rescted from mice also demonstrated the high expression of FAP in U87MG xenografts.

In the PET/CT imaging of human cancer patients, there existed several differences compared with micro PET/CT imaging with mice. Firstly, the high uptake in the gallbladder of mice was not appreciable in several human patients, which might because the fasting of mice will promote the secretion of bile, while eating in some human

patients might accelerate the removal of gallbladder contents, hence the difference of SUVmean in human gallbladder was not significant between Al^{18}F-NOTA-FAPI and 2-[^{18}F]FDG PET/CT imaging. Secondly, in the PET/CT imaging of most human cancer patients, similar to 2-[^{18}F]FDG, uptake of Al^{18}F-NOTA-FAPI in the bone was not significant (SUVmean = 0.7 ± 0.2), we ascribe such phenomenon to the lower expression level of FAP in human bone structure. Although in small animal biodistribution experiment, the accumulation of FAPI probes were relatively high. Furthermore, the low SUVmean in the bone cortex and bone marrow of patients would indicating the superior biostability of Al^{18}F-NOTA-FAPI in human body. In our previous clinical translational study utilizing the Al^{18}F-PSMA-BCH probe, the SUVmean were also low in the PET/CT imaging of prostate cancer patients [20]. Taken together, Al^{18}F-NOTA conjugate radiolabeled probes hold great feasibility and potential for clinical translational studies.

In the PET/CT imaging of several patients enrolled in this study, Al^{18}F-NOTA-FAPI was able to detect more tumour lesions compared with 2-[^{18}F]FDG, and was able to differentiate benign from malignant, thus can provide more effective information for the clinical treatment decisions of patients. As indicated in Fig. S7 and Table S3, primary tumour lesions of all patients showed high SUVmax in Al^{18}F-NOTA-FAPI PET/CT imaging, while in several patients (No. 4, 5 and 8), the SUVmax was much lower in 2-[^{18}F]FDG PET/CT imaging, which might result in pseudo-negative diagnosis in these patients. However, in the Al^{18}F-NOTA-FAPI PET/CT imaging of several patients (No. 1, 2, 3 and 9), primary tumour lesions showed lower SUVmax and SUVmean than that in 2-[^{18}F]FDG PET/CT imaging, which might remind us not to overestimate the tumour diagnosing efficacy of FAPI probes versus 2-[^{18}F]FDG. In this study, the differences of SUVmax and SUVmean in primary tumours were not significant between Al^{18}F-NOTA-FAPI and 2-[^{18}F]FDG PET/CT imaging, this was not surprising since the differences of the uptake in primary tumours between ^{68}Ga-DOTA-FAPI-04 and 2-[^{18}F]FDG PET/CT imaging of several cancer types were also not significant, as demonstrated by Chen et al [23]. However, when comparing the SUVmean values in primary tumours and normal organs, Al^{18}F-NOTA-FAPI showed

higher tumor-to-background ratios than 2-[^{18}F]FDG thanks to its low uptake in normal organs, especially in the spleen and brain. Therefore, Al^{18}F-NOTA-FAPI was a promising candidate and alternative to ^{68}Ga-DOTA-FAPI-04 for the popularization and application of FAPI PET/CT in clinical tumour imaging territory, and might act as supplementary to 2-[^{18}F]FDG PET/CT imaging, to provide more helpful informations for the precision diagnostic of individual patient.

Conclusion

In the present study, we developed the Al^{18}F-NOTA-FAPI probe for fibroblast activation protein targted imaging. Al^{18}F-NOTA-FAPI can be achieved under convenient manual operation with high radiolabeling yield and specific activity. NOTA-FAPI in this study showed higher affinity with FAP compared with several other FAPI probes. Al^{18}F-NOTA-FAPI showed excellent imaging efficacy in U87MG tumour bearing mice and was successfully translated into the clinical PET/CT imaging of cancer patients. Furthermore, Al^{18}F-NOTA-FAPI can be achieved by batch of production with high radioactivity using automatic synthesis, render it a promising candidate and alternative to ^{68}Ga-DOTA-FAPI-04.

Compliance with ethical standards

Conflicts of interest: The authors declare that they have no conflict of interest.

Ethics approval: All procedures involving human participants were carried out in accordance with the Ethics Committee of Peking University Cancer Hospital (2019 KT95), and registered in Chinese Clinical Trial Registry (ChiCTR2000038080). All animal studies were performed according to a protocol approved by the Peking University Cancer Hospital Animal Care and Use Committee.

Informed consent: Written informed consents were obtained from all participants included in the study.

Funding: This work was supported by National Natural Science Foundation of China projects No. 81871386 and 81871387, Yangfan project No. ZYLX201816, Dengfeng project No. DFL20191102, and Science Foundation of Peking University Cancer Hospital-2020-18.

References

1. Liu R, Li H, Liu L, Yu J, Ren X. Fibroblast activation protein: a potential therapeutic target in cancer. Cancer Biol Ther. 2012;13:123–9.
2. Kalluri R. The biology and function of fibroblasts in cancer. Nat Rev Cancer. 2016; 16:582–98.
3. Sánchez-Garrido MA, Habegger KM, Clemmensen C, Holleman C, Müller TD, Perez-Tilve D, et al. Fibroblast activation protein (FAP) as a novel metabolic target. Mol Metab. 2016;5:1015–24.
4. Teichgräber V, Monasterio C, Chaitanya K, Boger R, Gordon K, Dieterle T, et al. Specific inhibition of fibroblast activation protein (FAP)-alpha prevents tumor progression in vitro. Adv Med Sci. 2015; 60:264–72.
5. Chen M, Lei X, Shi C, Huang M, Li X, Wu B, et al. Pericyte-targeting prodrug overcomes tumor resistance to vascular disrupting agents. J Clin Invest. 2017;127:2689–701.
6. Wang J, Li Q, Li X, Yuan W, Huang S, Cai S, et al. A novel FAPα-based Z-Gly-Pro epirubicin prodrug for improving tumor-targeting chemotherapy. Eur J Pharmacol. 2017;815:166–72.
7. Scott AM, Wiseman G, Welt S, Adjei A, Lee FT, Hopkins W, et al. A phase I dose-escalation study of Sibrotuzumab in patients with advanced or metastatic fibroblast activation protein-positive cancer. Clin Cancer Res. 2003;9:1639–47.
8. Wang LS, Lo A, Scholler J, Sun J, Majumdar RS, Kapoor V, et al. Targeting fibroblast activation protein in tumor stroma with chimeric antigen receptor T Cells can inhibit tumor growth and augment host immunity without severe toxicity.

Cancer Immunol Res. 2014;2:154–66.

9. Loeffler M, Krüger JA, Niethammer AG, Reisfeld RA. Targeting tumor-associated fibroblasts improves cancer chemotherapy by increasing intratumoral drug uptake. J Clin Invest. 2006;116:1955–62.
10. Lee J, Fassnacht M, Nair S, Boczkowski D, Gilboa E. Tumor immunotherapy targeting fibroblast activation protein, a product expressed in tumor-associated fibroblasts. Cancer Res. 2005;65:11156–63.
11. Jansen K, Heirbaut L, Verkerk R, Cheng JD, Joossens J, Cos P, et al. Extended structure-activity relationship and pharmacokinetic investigation of (4-quinolinoyl)glycyl-2-cyanopyrrolidine inhibitors of fibroblast activation protein (FAP). J Med Chem. 2014;57:3053–74.
12. Lindner T, Loktev A, Altmann A, Giesel F, Kratochwil C, Debus J, et al. Development of quinoline-based theranostic ligands for the targeting of fibroblast activation protein. J Nucl Med. 2018;59:1415–22.
13. Kratochwil C, Flechsig P, Lindner T, Abderrahim L, Altmann A, Mier W, et al. ^{68}Ga-FAPI PET/CT: tracer uptake in 28 fifferent kinds of cancer. J Nucl Med. 2019;60:801–5.
14. Lindner T, Altmann A, Krämer S, Kleist C, Loktev A, Kratochwil C, Giesel F, Mier W, Marme F, Debus J, Haberkorn U. Design and development of ^{99m}Tc-labeled FAPI tracers for SPECT imaging and ^{188}Re therapy. J Nucl Med. 2020;61:1507–13.
15. Watabe T, Liu Y, Kaneda-Nakashima K, Shirakami Y, Lindner T, Ooe K, et al. Theranostics targeting fibroblast activation protein in the tumor stroma: ^{64}Cu- and ^{225}Ac-labeled FAPI-04 in pancreatic cancer xenograft mouse models. J Nucl Med. 2020;61:563–9.
16. Giesel FL, Kratochwil C, Lindner T, Marschalek MM, Loktev A, Lehnert W, et al. ^{68}Ga-FAPI PET/CT: biodistribution and preliminary dosimetry estimate of 2 DOTA-containing FAP-targeting agents in patients with various cancers. J Nucl Med. 2019;60:386–92.
17. Sabri S, Patrick C, Felix MM. The battle on time, money and precision: Da[^{18}F] id vs. [^{68}Ga]liath. Eur J Nucl Med Mol Imaing. 2020;47:2944–6.

18. Giesel F, Adeberg S, Syed M, Lindner T, Jimenez LD, Mavriopoulou E, et al. FAPI-74 PET/CT using either ^{18}F-AlF or cold-kit ^{68}Ga-labeling: biodistribution, radiation dosimetry and tumor delineation in lung cancer patients. J Nucl Med. 2020; https://doi.org/10.2967/jnumed.120.245084.
19. Toms J, Kogler J, Maschauer S, Daniel C, Schmidkonz C, Kuwert T, et al. Targeting fibroblast activation protein: radiosynthesis and preclinical evaluation of an ^{18}F-labeled FAP inhibitor. J Nucl Med. 2020;61:1806–13.
20. Liu T, Liu C, Xu X, Liu F, Guo X, Li N, et al. Preclinical evaluation and pilot clinical study of Al^{18}F-PSMA-BCH for prostate cancer PET imaging. J Nucl Med. 2019;60:1284–92.
21. Mentlein R, Hattermann K, Hemion C, Jungbluth AA, Held-Feindt J. Expression and role of the cell surface protease seprase/fibroblast activation protein-α (FAP-α) in astroglial tumors. Biol Chem. 2011;392:199–207.
22. Loktev A, Lindner T, Burger EM, Altmann A, Giesel F, Kratochwil C, et al. Development of fibroblast activation protein-targeted radiotracers with improved tumor retention. J Nucl Med. 2019;60:1421–9.
23. Chen H, Pang Y, Wu J, Zhao L, Hao B, Wu J, et al. Comparison of [^{68}Ga]Ga-DOTA-FAPI-04 and [^{18}F] FDG PET/CT for the diagnosis of primary and metastatic lesions in patients with various types of cancer. Eur J Nucl Med Mol Imaging. 2020;47:1820–32.

Figure Captions

Fig. 1 Schematic illustration for the synthesis of Al^{18}F-NOTA-FAPI probe, and the information of eariler reported probes [^{18}F]FGlc-FAPI and FAPI-74 [18, 19]. Al^{18}F-NOTA-FAPI and [^{18}F]FGlc-FAPI shared the identical FAP affinity group, as depicted by blue rectangle

Fig. 2 a Tracer uptake in U87MG cells at different time point after adding of Al^{18}F-NOTA-FAPI (2 μCi). **b** Competitive binding of Al^{18}F-NOTA-FAPI in U87MG cells, the IC_{50} of NOTA-FAPI was calculated to be 1.73 ± 0.93 nM

Fig. 3 a Biodistribution of Al^{18}F-NOTA-FAPI in KM mice at different time points post injection (n = 3, 30 μCi per mouse i.v.). **b** Pharmacokinetic study of Al^{18}F-NOTA-FAPI in KM mice (n = 5, 100 μCi per mouse i.v.)

Fig. 4 a Biodistribution of Al^{18}F-NOTA-FAPI in U87MG tumour bearing BALB/c Nude mice (n = 3). The uptake of Al^{18}F-NOTA-FAPI in tumour decreased rapidly from 1 h to 4 h post-injection, and can be blocked by the co-injection of non-radiolabeled NOTA-FAPI (20 nmol). **b** Comparison of tracer uptake in the tumour of U87MG tumour bearing mice between ^{68}Ga-DOTA-FAPI-04 and Al^{18}F-NOTA-FAPI. * $p<0.05$, ** $p<0.01$, **** $p<0.0001$

Fig. 5 Micro PET imaging of Al^{18}F-NOTA-FAPI in **a** A549, **b** U87MG and **c** blocked U87MG tumour bearing mice. The white arrow indicates the tumour xenograft, and the red arrow indicates the gallbladder. **d** The immunohistochemical staining of A549 xenograft indicated low expression of FAP (20× amplification). **e** The immunohistochemical staining of U87MG xenograft indicated high expression of FAP in tumour (20× amplification)

Fig. 6 a Comparison of SUVmean values in normal organs between Al^{18}F-NOTA-FAPI and 2-[^{18}F]FDG PET/CT imaging. **b** Comparison of tumor/spleen and tumor/brain SUVmean ratios between Al^{18}F-NOTA-FAPI and 2-[^{18}F]FDG PET/CT imaging. * $p < 0.05$, ** $p < 0.01$, *** $p < 0.001$, **** $p < 0.0001$. n = 9 (patient No. 10 was excluded because the lacking of 2-[^{18}F]FDG PET/CT imaging)

Fig. 7 Comparison between 2-[^{18}F]FDG and Al^{18}F-NOTA-FAPI PET/CT imaging of the 64 years old female pancreas cancer patient No. 5. **a** Maximum intensity projection, **b** CT images and **c** PET/CT images of 2-[^{18}F]FDG imaging, the white arrow indicated the pancreas, which showed relatively low uptake of 2-[^{18}F]FDG (SUVmax = 2.7). **d** Maximum intensity projection, **e** CT images and **f** PET/CT images of Al^{18}F-NOTA-

FAPI imaging, the white arrow indicated extremely high uptake of Al^{18}F-NOTA-FAPI in the pancreas (SUVmax = 36.3)

Fig. 8 Comparison between 2-[^{18}F]FDG and Al^{18}F-NOTA-FAPI PET/CT imaging of the 59 years old female lung cancer patient No. 8. **a** Maximum intensity projection, **b** CT images and **c** PET/CT images of 2-[^{18}F]FDG imaging, the white arrow indicated the lesion in the left superior lobe, which showed low uptake of 2-[^{18}F]FDG (SUVmax = 1.3). **d** Maximum intensity projection, **e** CT images and **f** PET/CT images of Al^{18}F-NOTA-FAPI imaging, the white arrow indicated relatively high uptake of Al^{18}F-NOTA-FAPI in the lesion (SUVmax = 6.6), which was further validated as malignancy

Figures

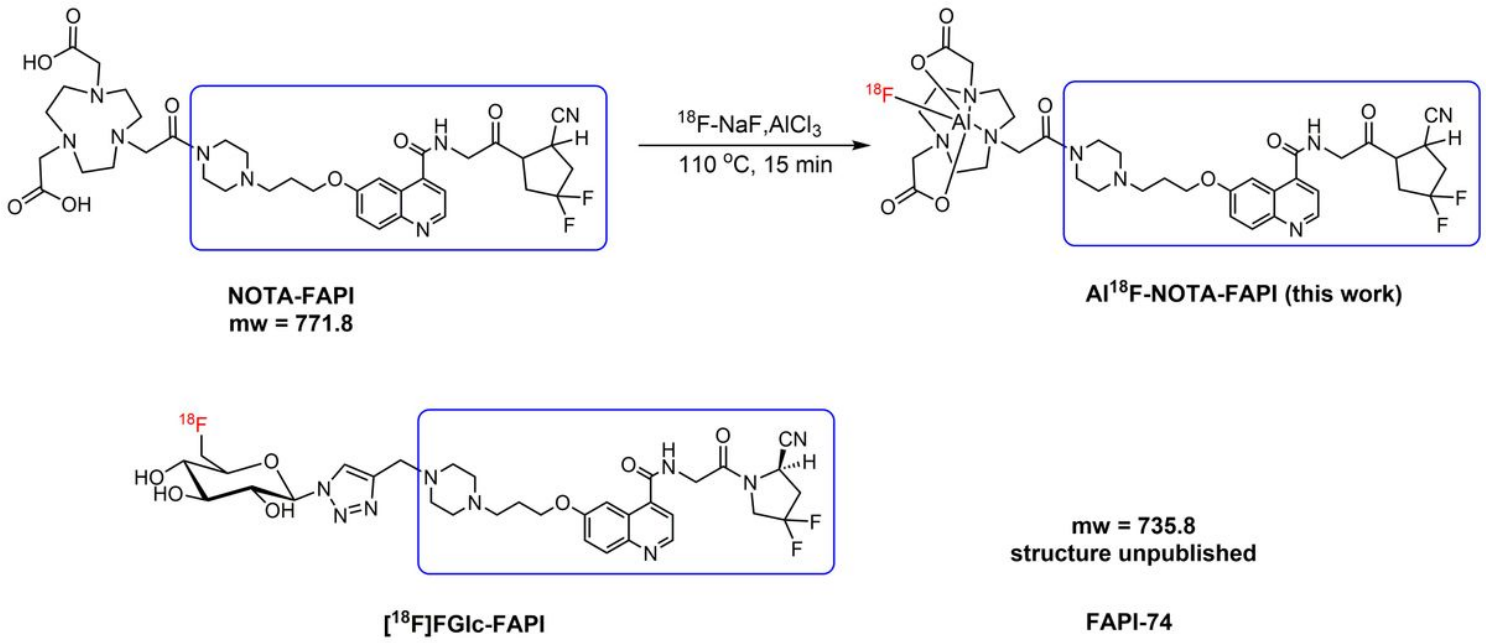

Figure 1

Schematic illustration for the synthesis of Al18F-NOTA-FAPI probe, and the information of eariler reported probes [18F]FGlc-FAPI and FAPI-74 [18, 19]. Al18F- NOTA-FAPI and [18F]FGlc-FAPI shared the identical FAP affinity group, as depicted by blue rectangle

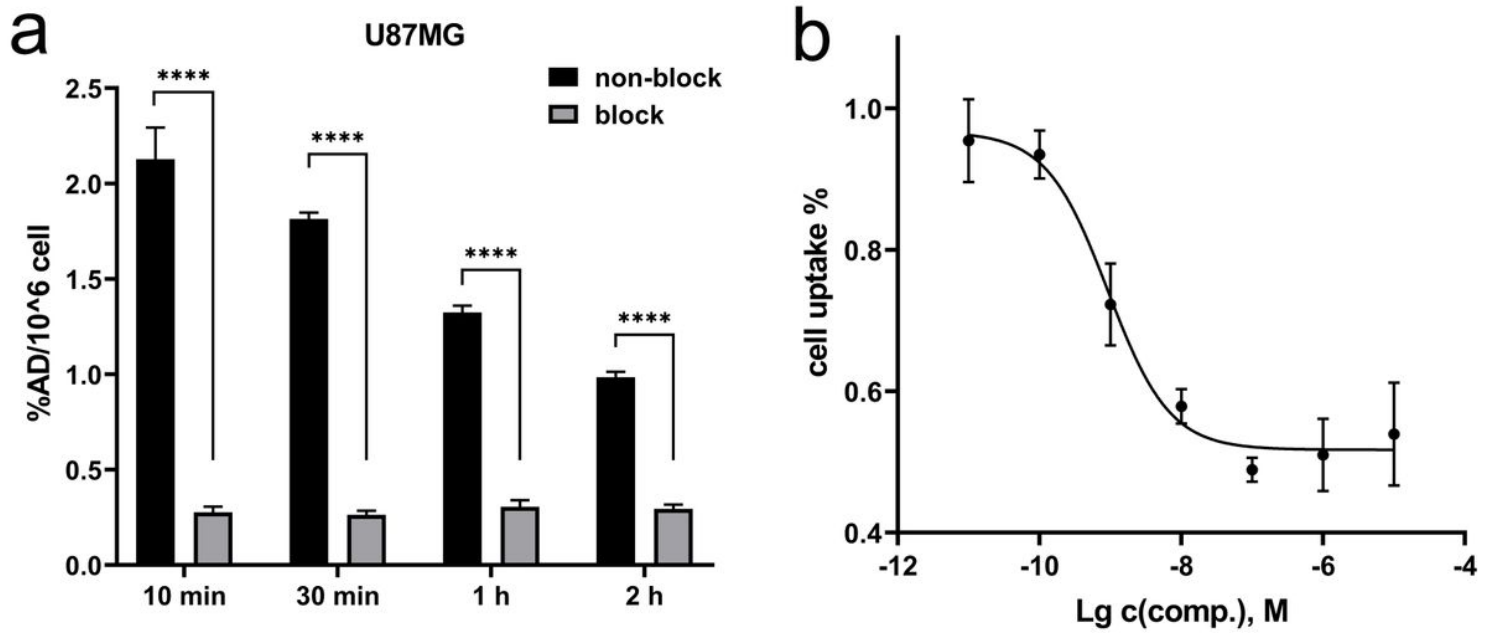

Figure 2

a Tracer uptake in U87MG cells at different time point after adding of Al18F- NOTA-FAPI (2 μCi). b Competitive binding of Al18F-NOTA-FAPI in U87MG cells, the IC50 of NOTA-FAPI was calculated to be

1.73 ± 0.93 nM

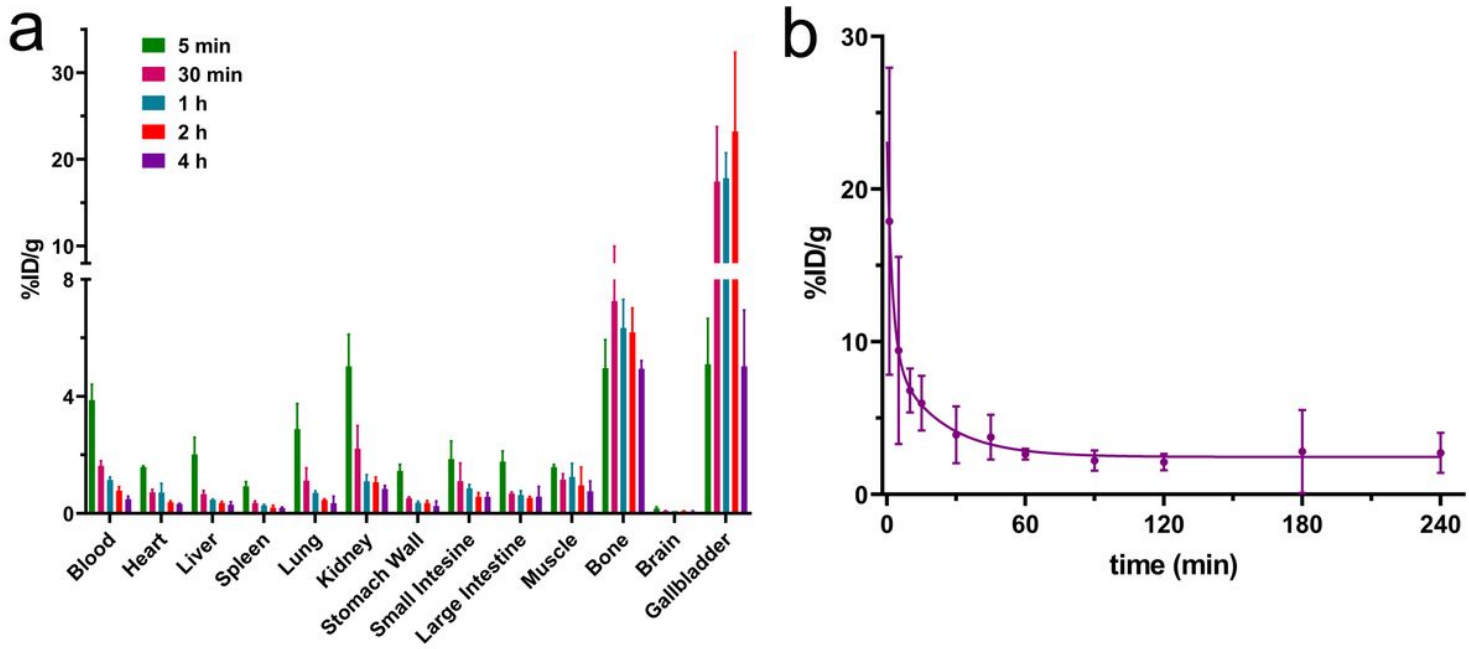

Figure 3

a Biodistribution of Al18F-NOTA-FAPI in KM mice at different time points post injection (n = 3, 30 μCi per mouse i.v.). b Pharmacokinetic study of Al18F-NOTA-FAPI in KM mice (n = 5, 100 μCi per mouse i.v.)

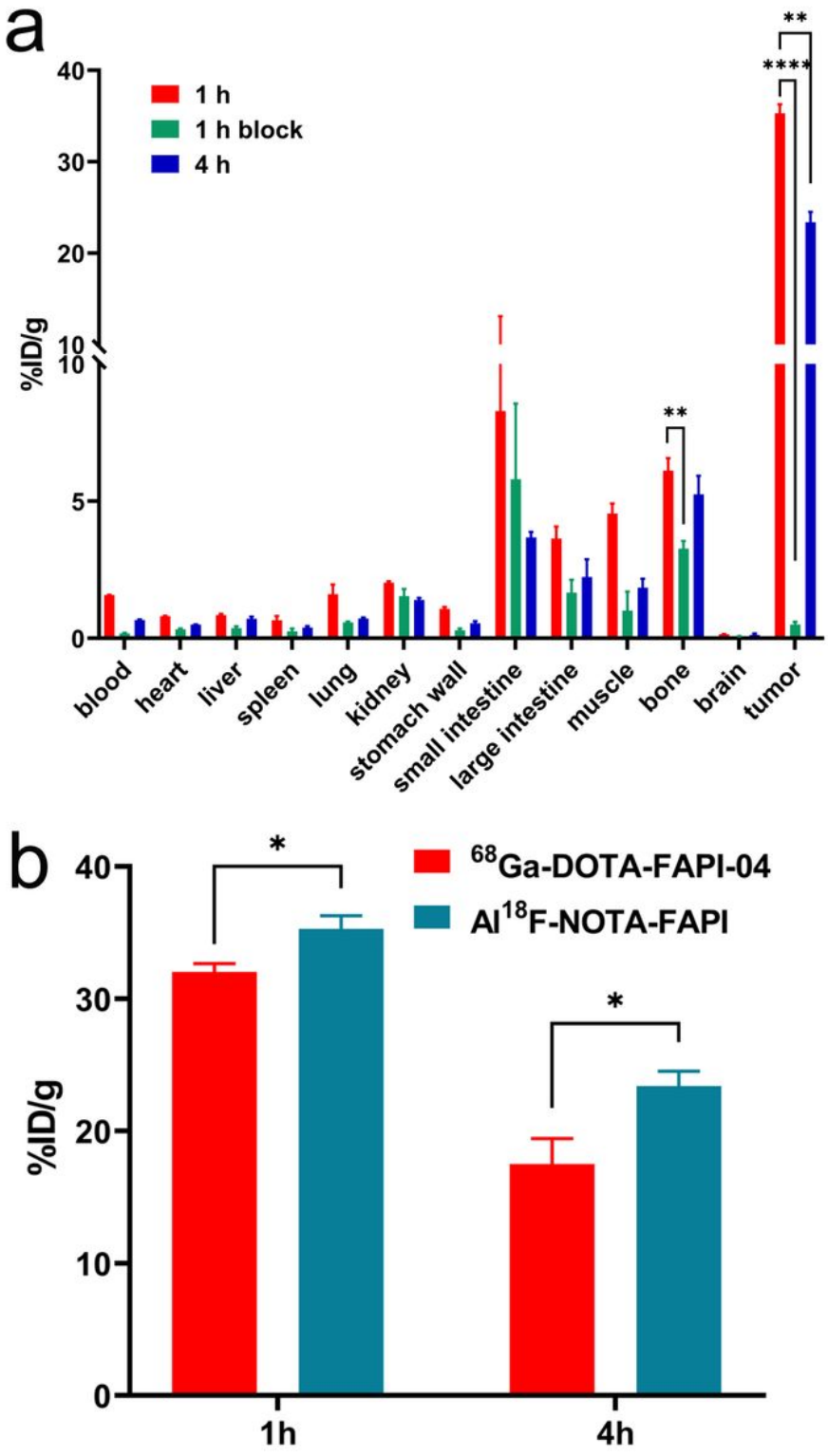

Figure 4

a Biodistribution of Al18F-NOTA-FAPI in U87MG tumour bearing BALB/c Nude mice (n = 3). The uptake of Al18F-NOTA-FAPI in tumour decreased rapidly from 1 h to 4 h post-injection, and can be blocked by the co-injection of non-radiolabeled NOTA-FAPI (20 nmol). b Comparison of tracer uptake in the tumour of U87MG tumour bearing mice between 68Ga-DOTA-FAPI-04 and Al18F-NOTA-FAPI. * $p<0.05$, ** $p<0.01$, **** $p<0.0001$

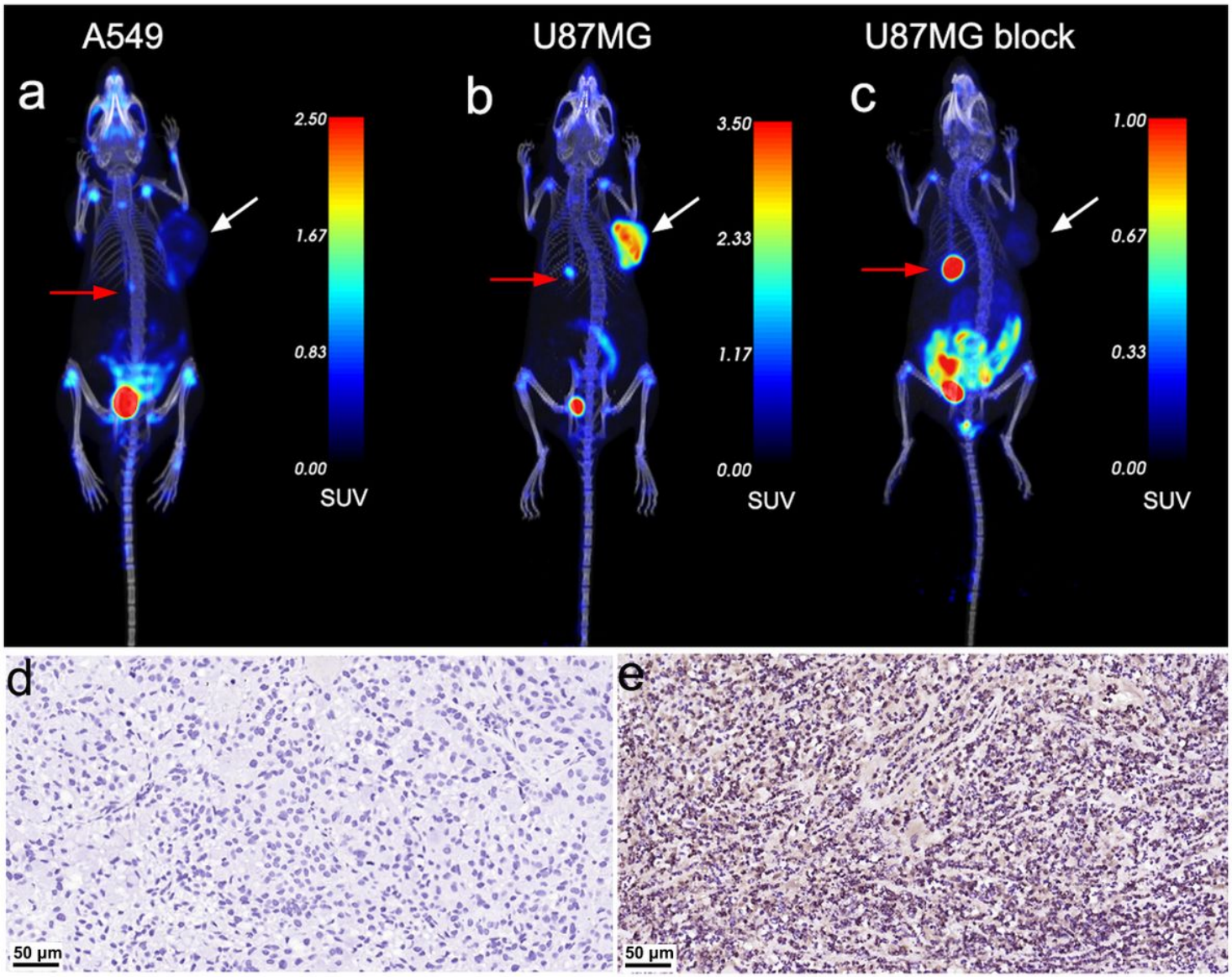

Figure 5

Micro PET imaging of Al18F-NOTA-FAPI in a A549, b U87MG and c blocked U87MG tumour bearing mice. The white arrow indicates the tumour xenograft, and the red arrow indicates the gallbladder. d The immunohistochemical staining of A549 xenograft indicated low expression of FAP (20× amplification). e The immunohistochemical staining of U87MG xenograft indicated high expression of FAP in tumour (20× amplification)

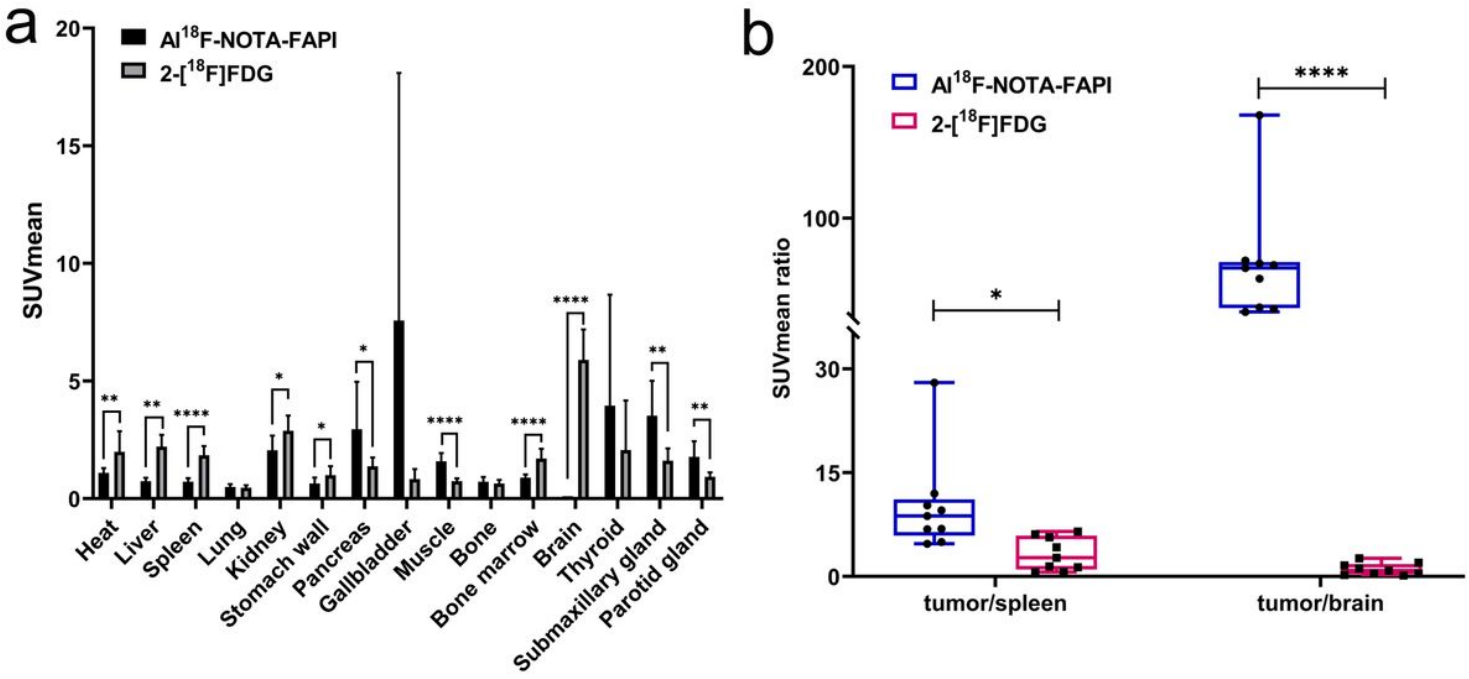

Figure 6

a Comparison of SUVmean values in normal organs between Al18F-NOTA-FAPI and 2-[18F]FDG PET/CT imaging. b Comparison of tumor/spleen and tumor/brain SUVmean ratios between Al18F-NOTA-FAPI and 2-[18F]FDG PET/CT imaging. * $p < 0.05$, ** $p < 0.01$, *** $p < 0.001$, **** $p < 0.0001$. n = 9 (patient No. 10 was excluded because the lacking of 2-[18F]FDG PET/CT imaging)

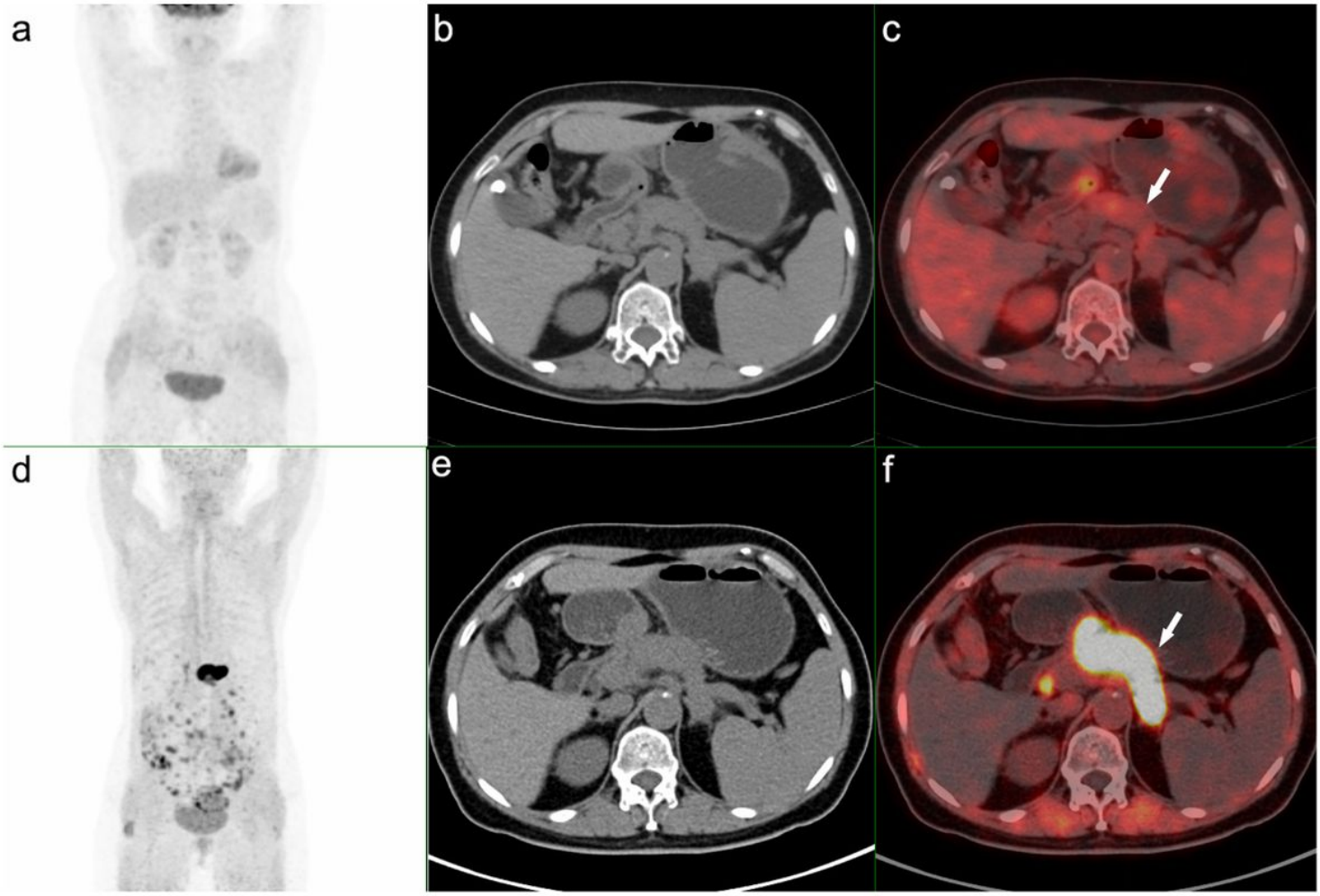

Figure 7

Comparison between 2-[18F]FDG and Al18F-NOTA-FAPI PET/CT imaging of the 64 years old female pancreas cancer patient No. 5. a Maximum intensity projection, b CT images and c PET/CT images of 2-[18F]FDG imaging, the white arrow indicated the pancreas, which showed relatively low uptake of 2-[18F]FDG (SUVmax = 2.7). d Maximum intensity projection, e CT images and f PET/CT images of Al18F-NOTA- FAPI imaging, the white arrow indicated extremely high uptake of Al18F-NOTA-FAPI in the pancreas (SUVmax = 36.3)

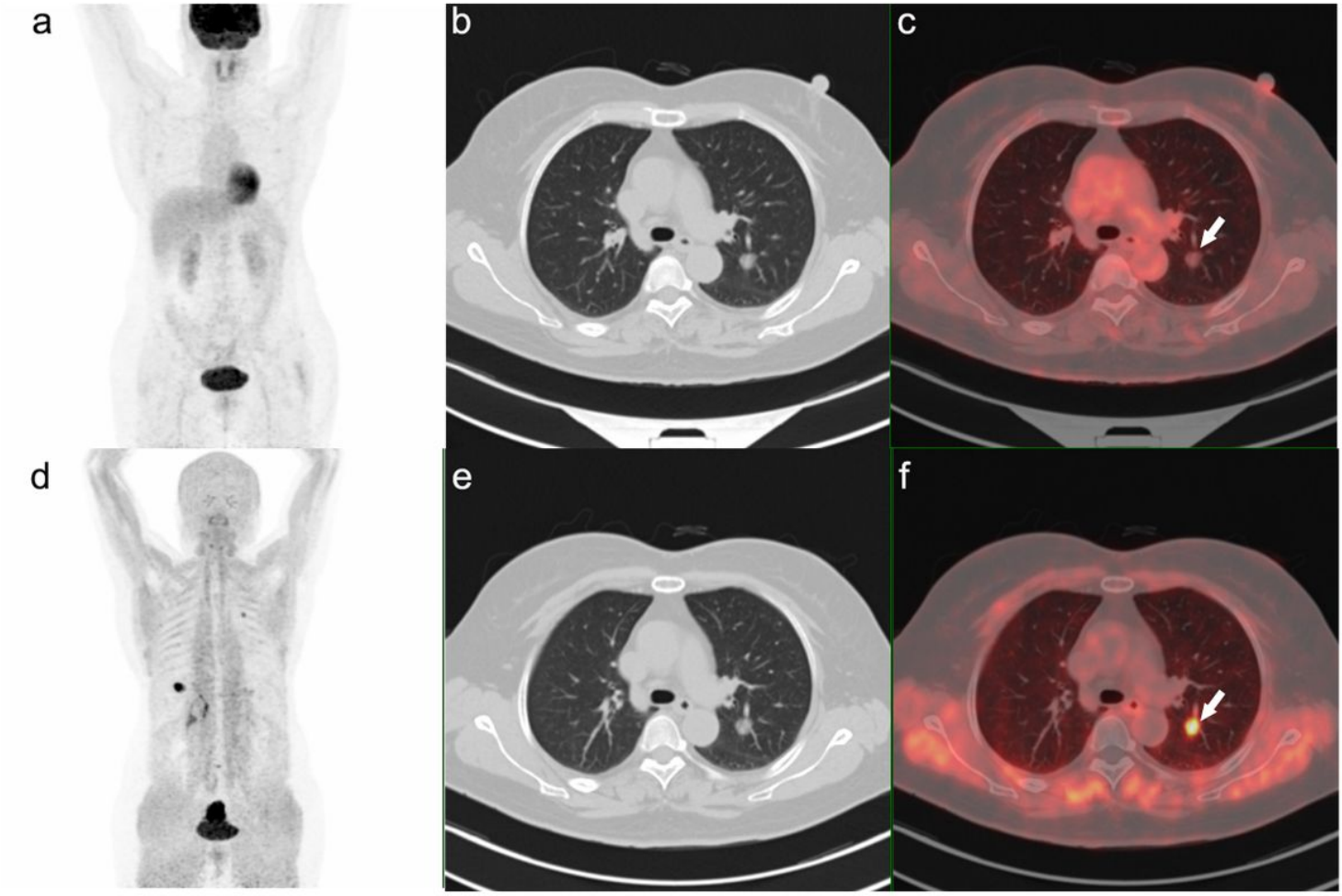

Figure 8

Comparison between 2-[18F]FDG and Al18F-NOTA-FAPI PET/CT imaging of the 59 years old female lung cancer patient No. 8. a Maximum intensity projection, b CT images and c PET/CT images of 2-[18F]FDG imaging, the white arrow indicated the lesion in the left superior lobe, which showed low uptake of 2-[18F]FDG (SUVmax = 1.3). d Maximum intensity projection, e CT images and f PET/CT images of Al18F-NOTA-FAPI imaging, the white arrow indicated relatively high uptake of Al18F-NOTA- FAPI in the lesion (SUVmax = 6.6), which was further validated as malignancy

Supplementary Files

This is a list of supplementary files associated with this preprint. Click to download.

- Tables.pdf
- Supplementarymaterial.pdf